Relative Rotor Phasing for Vibratory Load Minimization for a Coaxial Multicopter

Gaurav Makkar PhD Student
Robert Neimiec Research Scientist
Farhan Gandhi Redfern Chair, Director
Center for Mobility with Vertical Lift (MOVE)
Rensselaer Polytechnic Institute
Troy, NY United States

ABSTRACT

This study focuses on vibration reduction for a coaxial multicopter with 2-bladed, synchronized RPM, variable-pitch rotors through the use of rotor phasing. The study also examines the effect of aerodynamic interference between the rotors of a coaxial pair on the vibration predictions. A set of seven multi-rotor phase parameters are defined—a crossover azimuth for each the four coaxial pairs along with three aircraft level modes—pitch phasing, roll phasing, and differential phasing. The phase modes are examined in both a cross- and plus-configuration multicopter. Irrespective of whether interference was included or not, crossover azimuth of 0° tends to minimize the 2/rev lateral loads, while moderate values of crossover azimuth reduces the 2/rev longitudinal loads, for a coaxial rotor pair. For minimizing overall vibratory moments at the C.G., crossover azimuth corresponding to minimum 2/rev thrust is chosen for all the coaxial rotor pairs. It was observed that when interference is not included in the model, vibrations at the aircraft level are almost zero for pitch phasing and very low for the roll phase mode. However, when interference is included pitch phase is no longer a free parameter. With interference modeled, the 2/rev forces for the cross-configuration are $\sim 65\%$ lower than the plus-configuration, while the 2/rev moments are $\sim$ 70% lower.

NOTATION

Ω	Rotor RPM
ψ_C	Azimuth crossover (deg)
Φ_R	Roll phasing (deg)
Φ_P	Pitch phasing (deg)
Φ_D	Differential phasing (deg)
θ_k	Root Pitch of rotor k (deg)
θ_0	Collective pitch control(deg)

INTRODUCTION

Electric Vertical Takeoff and Landing (eVTOL) vehicles have seen massive growth in recent years. The simple design of the drive systems and flexibility afforded by electric power distribution have lowered the barriers to entry for eVTOL design. As a result, there has been a growing interest in scaling-up to much larger eVTOL aircraft, for both military use and commercial use including package delivery, and passenger transportation (Refs. 1, 2). Due to this simplicity and associated cost and maintenance benefits, fixed-pitch, variable RPM rotors have generally been utilized on eVTOL configurations.

One of the major challenges in the rotorcraft design is the vibration due to the cyclic rotor loads. With changing aerodynamic conditions on the blades over a revolution, the forces and moments experienced by a blade are harmonics of the rotational speed. Assuming identical blades in steady-state operation, vibratory loads at multiples of the blade passage frequency are passed to the airframe. The two-bladed rotors commonly used on eVTOL aircraft are likely to experience large vibrations, as the 1/rev oscillations in the dynamic pressure will introduce 2/rev drag, side force, pitching moment, and rolling moment in the nonrotating reference frame. The 2/rev changes in the aerodynamic conditions will also lead to 2/rev changes in rotor thrust and torque. Wind tunnel testing of eVTOL rotors revealed very large in-plane vibratory loads, with the 2/rev drag force greatly exceeding its steady value, acting on the same order as the mean rotor thrust (Ref. 3).

If the rotors of an eVTOL include variable-pitch for maneuvers, which may be necessary at passenger-carrying scales (Refs. 4, 5), then the variable-speed capability inherent to direct drive systems can be exploited to control their relative phasing . The use of relative phasing has been explored by Niemiec et al. (Refs. 6, 7) to reduce the vibrations for a classical quadcopter and octocopter. Schiller et al. (Ref. 8), Pascioni et al. (Ref. 9), and Smith et al. (Ref. 10) also utilized the concept of relative phasing of rotors to reduce the acoustic profile of different multicopter configurations.

Coaxial rotors are becoming common in both small and large multicopter configurations (Refs. 11, 12) because of the advantages like, reduction in the rotor diameter for a given gross weight since each rotor in the coaxial pair generates thrust to overcome the vehicle weight. For rotorcraft with coaxial rotors, interactions between the upper and lower rotors are important factors in design because the interactions have a sig-

Presented at the Vertical Flight Society's 78th Annual Forum & Technology Display, Ft. Worth, Texas, USA, May 10–12, 2022.

nificant effect on the inflow distribution.The goal of this paper is to explore the concept of rotor phase control for reduction in vibratory loads experienced by a multirotor aircraft with coaxial rotors and examine the effect of interference between rotors of the coaxial pair on the vibratory loads.

MODELING

The platform used in this study is a coaxial multicopter (X8, 2 coaxial rotors on each of the 4 booms) as shown in Fig. 1 and Fig. 2. The 4 kg aircraft is equipped with a variable-pitch derivative of the T-Motor 14x4.8 carbon fiber propellers. To facilitate phase-control, the rotors are assumed to spin at identical speeds, and collective-pitch control is used instead of variable-speed control to regulate rotor thrust. Other properties of the aircraft are listed in the Table 1.

Table 1: Summary of aircraft parameters

Parameters	Value
Rotor Radius	0.178 m (7 in)
Root Pitch	16.9°
Twist Rate	−8.38°
Boom length	0.325 m (12.8 in)
Rotor Speed	5000 RPM
GTOW	4 kg (8.8 lbs)
Vertical Separation between rotors	0.10 m (4.1 in)

The rotor analysis is performed using the Rensselaer Multicopter Analysis Code (RMAC, Ref. 13), a blade-element-theory-based multicopter analysis code. Rotors are treated either as isolated, or as interfering coaxial pairs. When the rotors are isolated, a 10-state Peters-He finite state dynamic wake model (Ref. 14) is utilized. The inflow dynamics take the form of Eq. 1.

$$M\overset{*}{\alpha}+VL^{-1}\alpha=\frac{1}{2}\tau \tag{1}$$

where α represents all of the inflow states. This equation is repeated for every rotor on the aircraft, and is phase-averaged over a revolution. When interference between coaxial rotor pairs is included, Pressure Potential Superposition Inflow Modeling (PPSIM, Ref. 15) is used to model the inflow between the rotors. The PPSIM equations of motion take the form of Eq. 2.

$$\begin{bmatrix} E_{LL} & E_{LU} \\ E_{UL} & E_{UU} \end{bmatrix}^{-1} \begin{bmatrix} \overset{*}{\alpha}_L \\ \overset{*}{\alpha}_U \end{bmatrix} + \begin{bmatrix} V_L & 0 \\ 0 & V_U \end{bmatrix} \begin{bmatrix} L_{LL} & L_{LU} \\ L_{UL} & L_{UU} \end{bmatrix}^{-1} \begin{bmatrix} \alpha_L \\ \alpha_U \end{bmatrix} = \frac{1}{2} \begin{bmatrix} \tau_L \\ \tau_U \end{bmatrix} \tag{2}$$

Expressions for the block elements of E and L are available in Ref. 15. Interference between different rotor pairs is neglected, though the PPSIM framework can be extended beyond coaxial rotor pairs. The rotor blades are assumed to be rigid, due to the stiffness of the carbon-fiber construction of the T-motor props. Once a trim condition is determined, periodic rotor loads are exported for post-processing into aircraft-level vibrations.

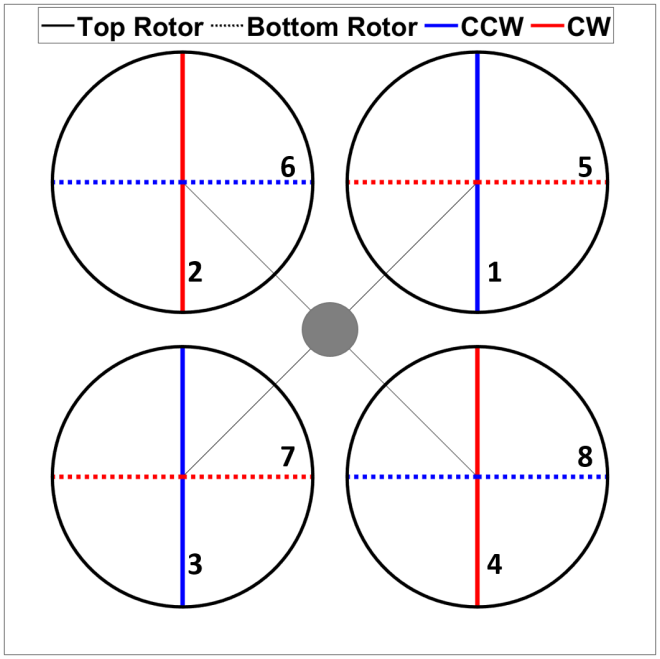

Figure 1: X8 configuration

Figure 2: RPI's X8 Platform

The azimuthal position of the rotors is an eight-dimensional space, and if one rotor is defined as a reference, the relative phase can be expressed using 7 parameters. For example, if rotor 1 in Fig. 1 is selected as the reference rotor, the degrees

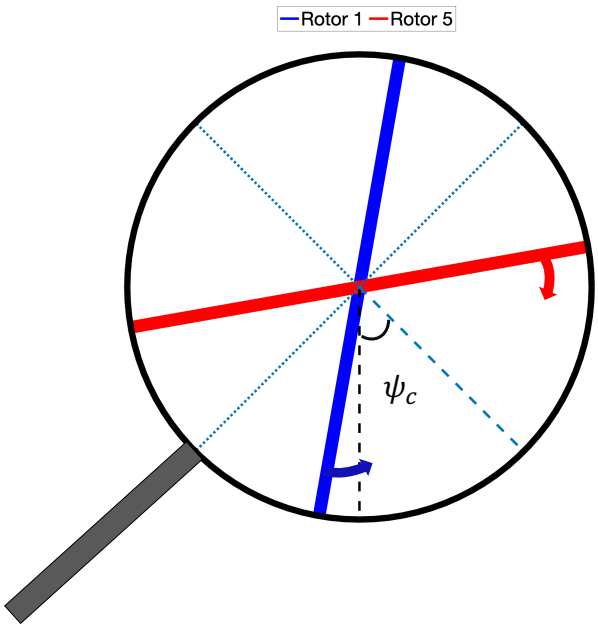

Figure 3: Coaxial rotor pair (rotor 1 and rotor 5)

of freedom may be expressed as

$$\phi_k = \psi_k - \psi_1 \qquad 2 \leq k \leq 8 \tag{3}$$

In this expression, ϕ_k is a free parameter that can be modified to adjust the phase of rotor k relative to rotor 1. Rotor 1's position then becomes a time-parameter, increasing constantly over time as the rotors spin.

Alternately, the relative phases of groups of rotors can be combined in meaningful ways to express the relative phasing of the rotors. For example, consider one coaxial pair of rotors, as shown in Fig. 3. Because this pair of 2-bladed rotors counter-rotate, the blades overlap four times per revolution, once in each quadrant. The crossover points can be manipulated by introducing relative phase between the upper and lower rotor. For every 2° rotor 1 leads rotor 5, the the crossover points move by 1° in the counter-clockwise direction. Arbitrarily, the first crossover point (as experienced by the upper rotor during a revolution) is selected as a free parameter. In pairs where the upper rotor spins counter-clockwise (as in Fig. 3), this corresponds to the rear-right quadrant. For pairs where the upper rotor spins clockwise, this crossover is on the rear-left quadrant. After defining the crossover point for each coaxial pair results, 4 of the 7 parameters become defined.

To define the remaining three phase parameters, the same aircraft-level "modes" used for the quadcopter in Ref. 6,7 are adapted for the coaxial quadrotor. As on the quadcopter, Φ_R (Fig. 4a) introduces a phase difference between the left and right rotors. On an X8, this manifests as a difference in the time at which the left and right rotors crossover. For positive Φ_R, when rotors on the right crossover, the rotors on the left have an angle of $4\Phi_R$ between them. Similarly, Φ_P represents a phase difference of the front rotors relative to the rear rotors, while Φ_D is a phase difference between adjacent pairs of rotors. Combined with the four crossover points, a complete set

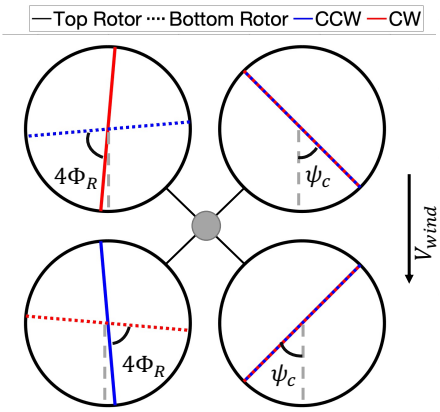

(a) Roll Phasing, Φ_R

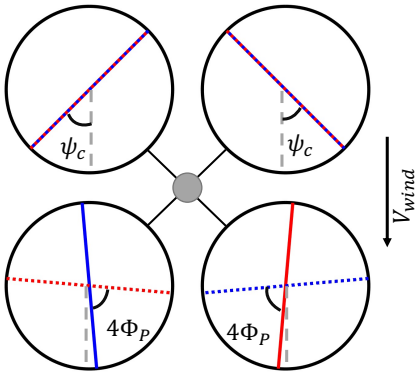

(b) Pitch Phasing, Φ_P

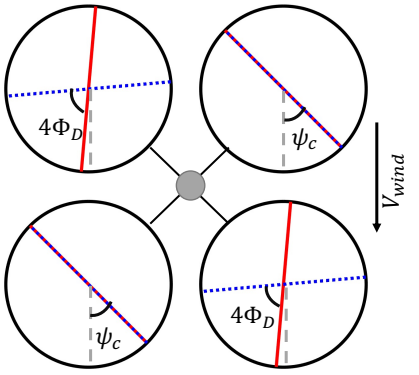

(c) Differential Phasing, Φ_D

Figure 4: Phasing Modes in Cross-Configuration

of multi-rotor phase parameters is formed.

The azimuthal position of any individual blade can be obtained through the multi-rotor phase parameters via Eq. 4. In addition to the seven phase parameters previously described, a time-parameter Φ_0, which contributes equally to each rotor's

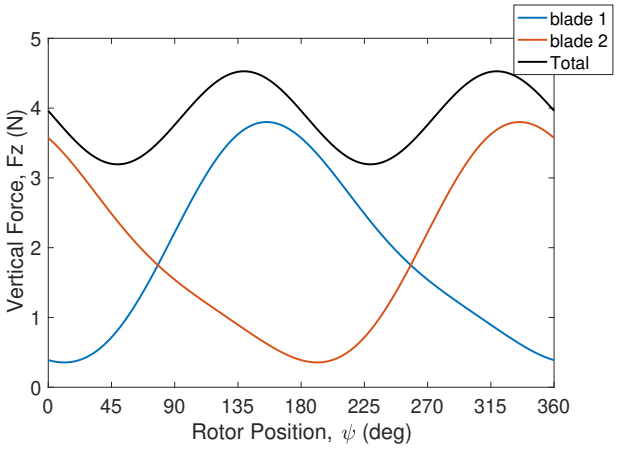

Figure 5: Blade root vertical shear for isolated rotor in edgewise flow

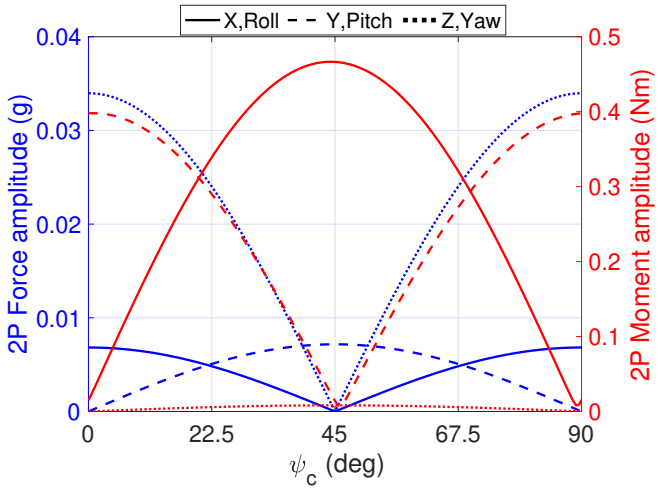

Figure 6: Amplitude of 2/rev vibratory forces for a coaxial rotor pair

azimuth, is defined. Naturally, Φ_0 does not affect the relative phase between the rotors, nor any of the vibratory loads.

$$\begin{bmatrix} \psi_1 \\ \psi_2 \\ \psi_3 \\ \psi_4 \\ \psi_5 \\ \psi_6 \\ \psi_7 \\ \psi_8 \end{bmatrix} = \begin{bmatrix} 1 & 0 & 0 & 0 & 1 & 1 & 1 & 1 \\ 0 & 1 & 0 & 0 & 1 & -1 & -1 & 1 \\ 0 & 0 & 1 & 0 & -1 & -1 & 1 & 1 \\ 0 & 0 & 0 & 1 & -1 & 1 & -1 & 1 \\ -1 & 0 & 0 & 0 & 1 & 1 & 1 & 1 \\ 0 & -1 & 0 & 0 & 1 & -1 & -1 & 1 \\ 0 & 0 & -1 & 0 & -1 & -1 & 1 & 1 \\ 0 & 0 & 0 & -1 & -1 & 1 & -1 & 1 \end{bmatrix} \begin{bmatrix} \psi_c^1 \\ \psi_c^2 \\ \psi_c^3 \\ \psi_c^4 \\ \Phi_P \\ \Phi_R \\ \Phi_D \\ \Phi_0 \end{bmatrix} \quad (4)$$

RESULTS

Isolated Rotor

No Interference For an edgewise rotor in forward flight, the freestream velocity produces a 1/rev variation in the tangential velocity seen by the blades, resulting in a variation in dynamic pressure. This results in a dominantly 1/rev blade root vertical shear, shown in Fig. 5 as a function of azimuth.

Coaxial Pair

Fig. 6 shows the 2/rev net boom tip forces and moments (from the combination of the upper and lower rotors on a single boom) when the ψ_c is increased from 0° to 90°. When $\psi_c = 0$, the upper and lower rotors cross the 90°-270° line simultaneously. Thus, both rotors experience maximum lift at the same time, as can be seen in Fig. 7 on the far left. Because the vibratory rotor thrust is in-phase, the 2/rev z-force amplitude (Fig. 6, dotted blue) is at a local maximum when $\psi_c = 0$. As ψ_c increases (moving rightward in Figs. 6 and 7), the upper/lower rotor thrusts become increasingly out-of-phase, and the 2/rev z-force amplitude drops. This continues until $\psi_c = 45°$ where the upper/lower rotors' thrusts are completely out-of-phase, and there are no 2/rev z-forces. The reverse trend occurs as ψ_c goes from 45° to 90°. Because the rotors are two-bladed, there is periodicity every $180°/N_{blades} = 90°$. Drag (blue solid) and pitching moment (red dashed) behave almost identically to the rotor thrust, with minima occuring at or near $\psi_c = 45°$, with similar interference patterns between the two rotors.

The side force (blue dashed), rolling moment (red solid), and yaw moment (red dotted) exhibit the opposite trend, with local maxima occurring at $\psi_c = 45°$ and minima occurring at $\psi_c = 0°$ or 90°. This occurs due to the fact that the rotors counter-rotate. When $\psi_c = 0°$, and the rotors cross the 90°--270° line, both experience their maximum rolling moments, but in opposite directions, ultimately canceling one another out. Conversely, for $\psi_c = 45$, one rotor reaches its minimum rolling moment (as it crossed the 0-180° line) while the other reaches its maximum, resulting in maximum vibratory load when the two rotors are summed. The arguments presented here are independent of the thrust produced by this rotor pair– as long as the upper and lower rotor produce the same thrust, the effect of ψ_c on the net vibratory loads of the rotor pair is the same.

On a cross-type quadcopter, the two front rotors' lateral forces/moments cancel one another out, as long as they are in-phase (Ref. 7). Similarly, the two front rotor pairs of rotors in an X8 will also cancel one another's lateral forces at the aircraft level. Thus, the crossover point is selected to minimize the longitudinal vibratory loads, $\psi_c = 45°$. This phasing will be used for all coaxial pairs, when interference is neglected.

PPSIM Interference In a similar process to the coaxial rotor pair without interference, ψ_c is varied within a single rotor pair to explore the effect interference has on the vibratory loads produced by said rotor pair. Like the interference-off case, the upper and lower rotors are trimmed to produce the same steady thrust. Unlike the interference-off case, the trends are not independent of the overall rotor thrust. Figs. 8 and 9 show the 2/rev vibratory forces and moments for a coaxial rotor pair trimed to 7.6N and 11.9N of total thrust, respec-

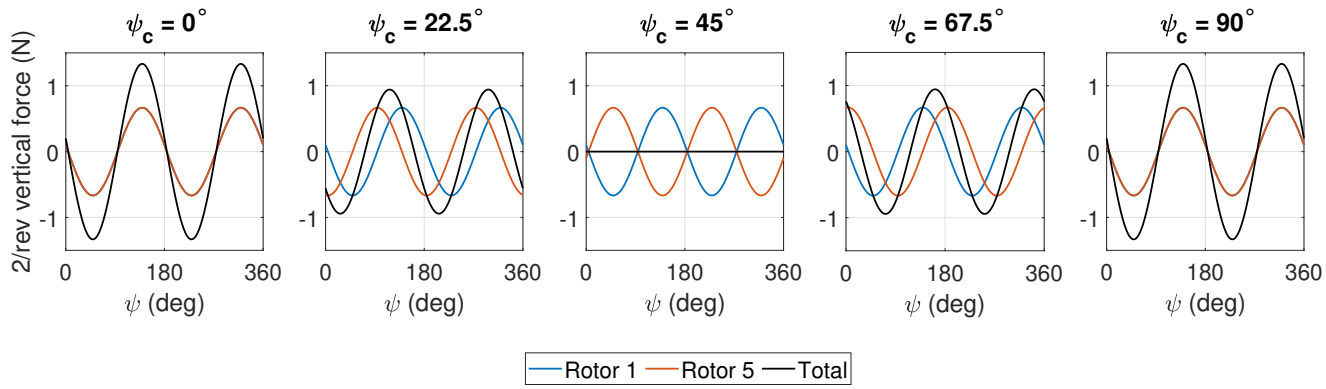

Figure 7: 2/rev vibratory vertical force for the coax pair (Rotor 1 and Rotor 5)

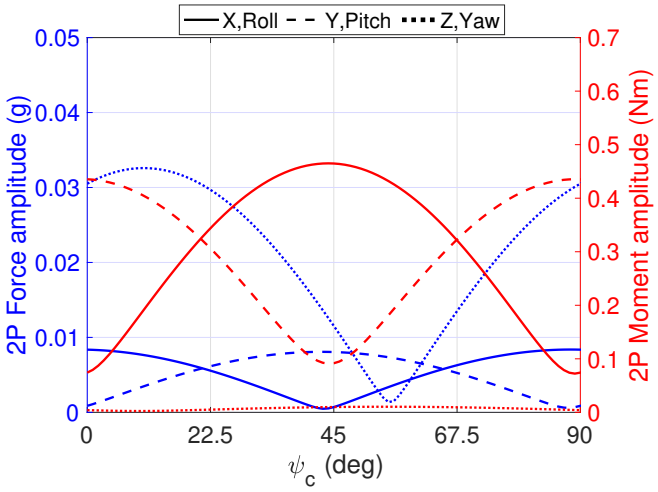

Figure 8: Amplitude of 2/rev Vibratory Forces and Moments for coaxial rotor pair (Rotor 1 and 5) with interference

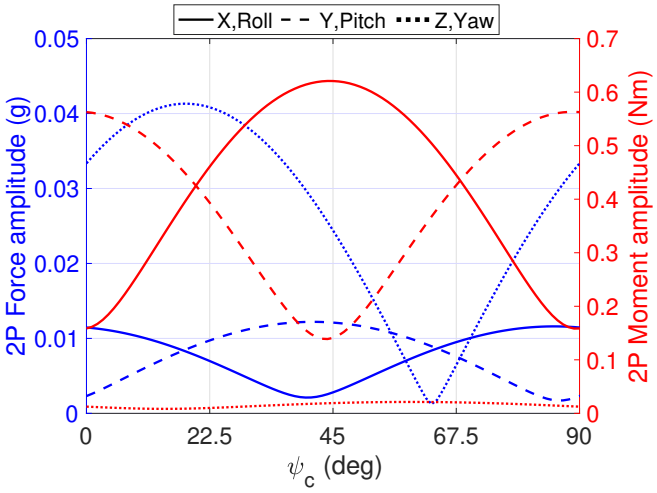

Figure 9: Amplitude of 2/rev Vibratory Forces and Moments for coaxial rotor pair (Rotor 4 and 8) with interference

tively. These values are consistent with pitch moment balance on the cross-type X8 pictured in Fig. 2. Some of the loads (drag, side force, pitch moment) exhibit qualitatively similar behavior to the interference-off case, though values are generally higher than they were in interference-off cases, there are large differences in the thrust, roll moment, and yaw moment.

In particular, the 2/rev thrust cannot be completely canceled, though it can be brought very low within a rotor pair. However, the crossover point at which the 2/rev thrust is minimized is not constant at different thrust levels. Fig. 10a and Fig. 10b show the interaction of vibratory thrust for the coaxial rotor pair of rotor 1 and 5, and rotor pair of rotor 4 and 8. Unlike interference-off case (Fig. 7, 2/rev thrust is not in-phase for $\psi_c = 0°$, and also these vibratory loads don't cancel at $\psi_c = 45°$). Comparing Figs. 8 and 9, it seems that increasing the thrust produced by this rotor pair results in an increase in the minimizing ψ_c.

Because vibratory thrust will produce large moments at the center of gravity (0.1g corresponds to 1.27 Nm of moment), as well as substantial shear and bending loads on the structure, it is desirable to reduce the 2/rev thrust, even at the expense of the other forces and moments. This, coupled with the fact that the left/right sides symmetry will still cancel lateral vibratory loads at the C.G. suggests that a crossover point that minimizes thrust is a good strategy for reducing aircraft-level vibrations.

Cross Configuration - No Interference

In forward flight, the multicopter must pitch nose-down to vector its thrust forward to overcome aerodynamic drag. Additionally, due to the nose-up pitching moment that is produced by the rotors due to the longitudinal inflow distribution, the rear rotors must operate at a higher root pitch than the front rotors. Due to the symmetry of the vehicle, the left and right sides are identical to one another. Trim values for the pitch attitude and rotor collective pitch are presented in Table 2.

Roll Phasing While holding $\psi_c = 45°$ for all rotors, consider positive roll phasing (Φ_R), illustrated in Fig. 4a. The right rotors will lead an imaginary reference blade and the left rotors will lag, which manifests as a phase delay between the

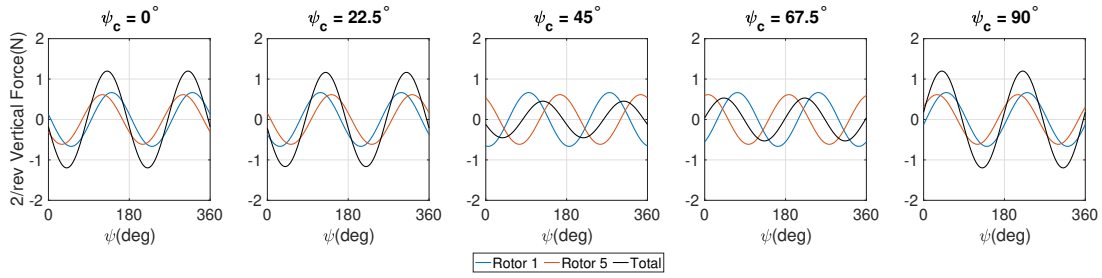

(a) 2/rev vibratory vertical force for coaxial pair (Rotor 1 and Rotor 5)

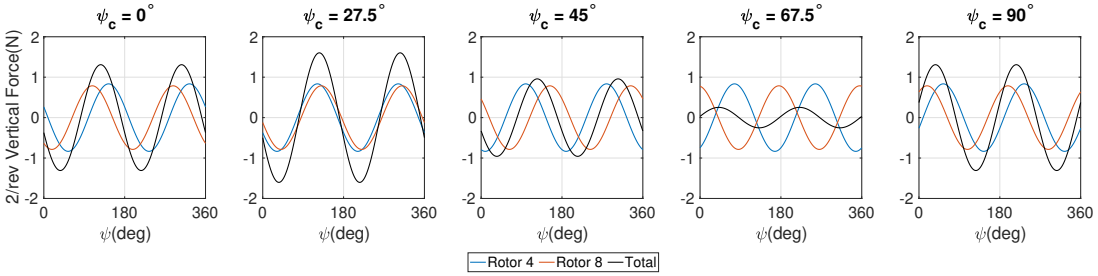

(b) 2/rev vibratory vertical force for coaxial pair (Rotor 4 and Rotor 8)

Figure 10: 2/rev vertical force for coaxial pairs with interference

Table 2: Trim at 10m/s – Cross Configuration Without Interference Modeling

Parameter	Value
Pitch attitude	$-3.02°$
Front rotor collective	$8.7°$
Rear rotor collective	$10.2°$

crossover points for the left/right rotors. When the rotors on the right cross over, the rotors on the left form an angle of $4\Phi_R$ between them. Because the crossover of the two right (or two left) rotor pairs are simultaneous, these pairs are referred to as "in-phase" for the remainder of this study.

Figure 11 shows the 2/rev rolling moment about the vehicle C.G. for different values of Φ_R ($\Phi_P = \Phi_D = 0$). Generally, this rolling moment is from two sources: 2/rev hub rolling moments from each pair of rotors, and a 2/rev thrust, acting with a moment arm. Because $\psi_c = 45°$, the 2/rev thrust generated by each rotor pair is zero. Thus, the rolling moments about the C.G. are entirely due to hub rolling moments. Each rotor on the left side of the vehicle (e.g. top-front-left) has a counterpart on the right side of the vehicle (e.g. top-front-right) that is identical, except for the spin direction, the lateral forces/moments cancel at the aircraft level. This is shown in Fig. 11 on the far left (or far right), where the 2/rev rolling moments generated by the rotors on the left side of the vehicle (red dashed) is out-of-phase with those generated by the right side of the vehicle (blue solid) when $\Phi_R = 0°$ (or $\Phi_R = 90°$). As Φ_R deviates from zero, the rolling moments generated on the left/right sides are increasingly in-phase, with a maximum occurring at $\Phi_R = 45°$.

The amplitude of the 2/rev rolling moment, along with all of the other forces/moments at the C.G. are plotted versus Φ_R in Fig. 12. Like the rolling moment, the 2/rev side force and yaw moment are cancelled at $\Phi_R = 0°, 90°$, and are maximized at $\Phi_R = 45°$. Notably, the 2/rev longitudinal forces and moments are zero for all Φ_R, as the 2/rev thrust, drag, and hub pitching moments cancel within each coaxial pair. Further, because the 2/rev rotor thrust cancels within a rotor pair, the 2/rev thrust-induced moments will also cancel, allowing for near-zero 2/rev loads in all axes, which was not achievable on a quadrotor (Ref. 7).

Pitch Phasing Next, consider positive pitch phasing (Fig. 4b), which causes the front rotors to lag and the rear rotors to lead relative to a reference blade, causing a phase delay between the crossover of the front/rear pairs of rotors. Fig. 13 shows the 2/rev forces and moments for pitch phasing (Φ_P) between $0°$ to $90°$. For any value of Φ_P the front rotor pairs are in-phase with one another, as are the two rear rotor pairs. Consequently, the lateral forces and moments generated by the front/rear rotor quartets mostly or entirely cancel out. As the longitudinal 2/rev forces (thrust, drag, and pitching moment) are cancelled within each coaxial pair, they remain 0 regardless of the value of Φ_P. Because the 2/rev forces and moments are practically zero for all Φ_P, it may be used freely to either influence the acoustic profile of the vehicle, or reduce higher-harmonic vibrations.

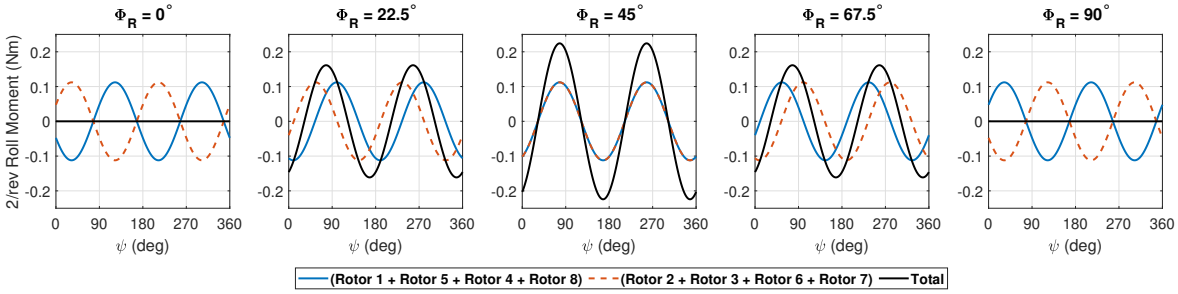

Figure 11: 2/rev rolling moment at aircraft C.G. using roll phasing

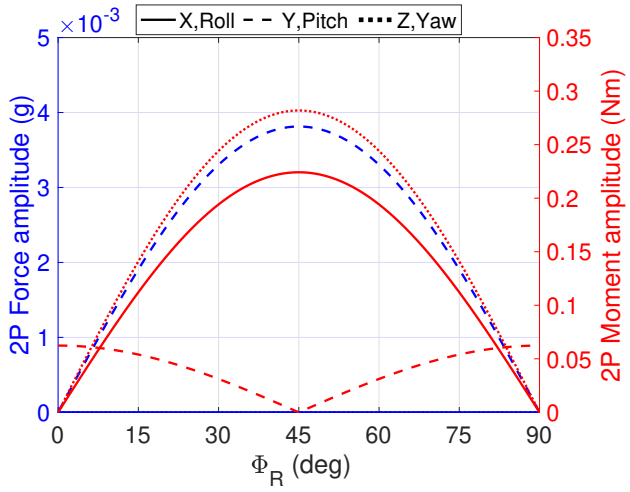

Figure 12: Amplitude of 2/rev vibratory forces and moments at aircraft C.G using Roll Phasing ,Φ_R

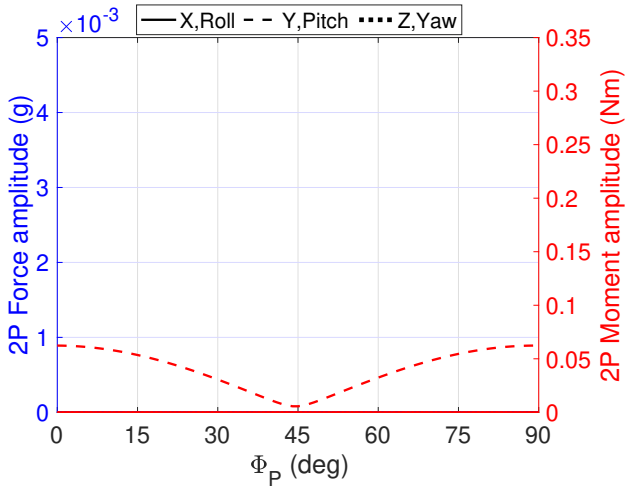

Figure 13: Amplitude of 2/rev vibratory forces and moments at aircraft C.G using Pitch Phasing ,Φ_P

Differential Phasing For differential phasing (Φ_D), the coaxial pairs on front-right and rear-left lead and the remaining rotor pairs lag relative to a reference blade (Fig. 4c). Thus, there is a delay between the crossovers of the front-right+rear-left and the front-left+rear-right rotor pairs. The 2/rev forces and moments at the aircraft C.G. for different values of Φ_D are shown in Fig. 14. Similar to Φ_P and Φ_R, the longitudinal forces and moments are zero regardless of the differential phasing. Qualitatively, the 2/rev forces and moments behave similarly with Φ_D as they did with Φ_R, though at a much larger amplitude. The vibratory loads with differential phasing are enormous (8-10×) near $\Phi_D = 45°$, relative to $\Phi_R = 45°$. This is because, at $\Phi_D = 45°$, the side force/rolling moment magnitude of all the rotors interfere constructively, whereas for $\Phi_R = 45°$, there was partial cancellation between front-right/rear-right pairs (as well as the front-left/rear-left pairs) but there is no cancellation whatsoever for $\Phi_D = 45°$.

Cross-Configuration - Interference

Table 3: Cross-configuration - Trim at 10m/s With Interference Modeling

Parameter	Value
Pitch Attitude	$-3.38°$
Front-Top Collective	$9.31°$
Rear-Top Collective	$11.0°$
Front-Bottom Collective	$9.57°$
Rear-Bottom Collective	$11.7°$

Due to the steady effects of interference, the vehicle must be

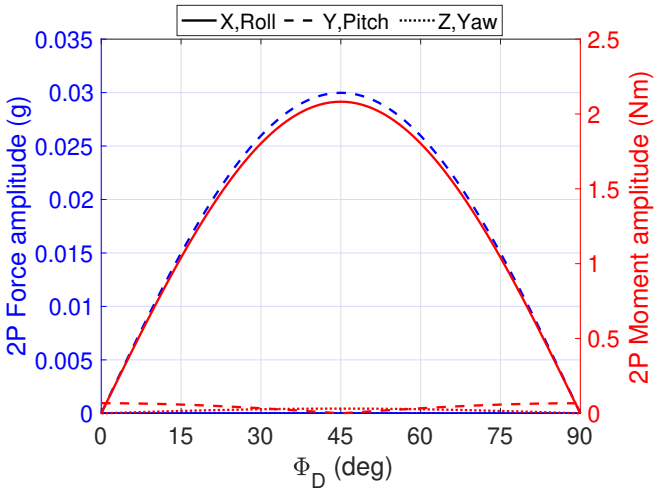

Figure 14: Amplitude of 2/rev vibratory forces and moments at aircraft C.G using Differential Phasing ,Φ_D

retrimmed when the interference model is activated. Additionally, the upper/lower rotors within a rotor pair are constrained to produce the same thrust, in addition to the typical trim equations The resulting trim solution is presented in Table 3. The most obvious change is that the upper and lower rotors no longer operate at the same collective, with the lower rotors consistently operating at higher collective than the upper rotors. The next most significant change is that the collective is overall higher, due to the extra downwash over each rotor due to the interference. In accordance with the previously stated vibration-minimization strategy, ψ_c is selected such that 2/rev thrust is cancelled to the greatest extent possible within a rotor pair, and thus $\psi_c = 54^\circ$ for the front rotors, and 63° for the rear rotors.

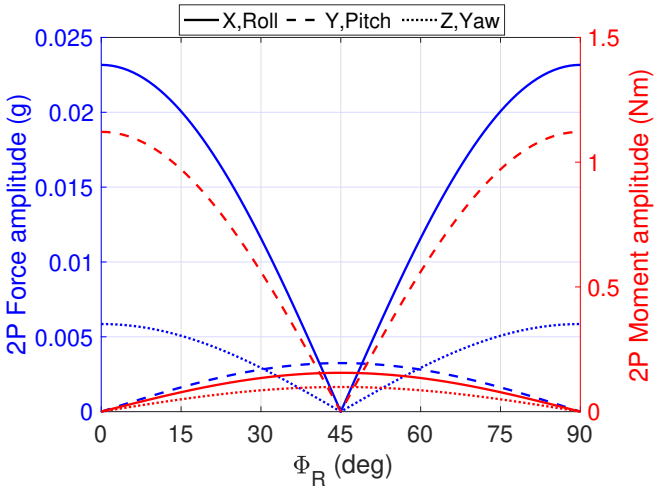

Figure 15: Amplitude of 2/rev vibratory forces and moments at aircraft C.G. using Φ_R with interference modeling

The 2/rev forces and moments at the C.G. as Φ_R is swept from 0° to 90° are plotted in Fig. 15. Qualitatively speaking, the curves are similar to the zero-interference case, but with a much greater 2/rev force amplitude (compare the scales of Figs. 12 and 15). This suggests that the force/moment interference patterns are not markedly different when aerodynamic interference is present. Fig. 16 shows the 2/rev drag and 2/rev side force for $\Phi_R = 45^\circ$. For the drag, it is clear that the two pairs of front rotors are out-of-phase, as are the 2/rev drag produced by the two rear pairs. Consequently, 2/rev drag is completely cancelled. A similar trend occurs for the thrust and pitching moment. For the side force, the two front pairs are in-phase with each other, but out-of-phase with the rear pairs, leading to destructive interference, but not complete cancellation, with similar effects occurring for rolling and yawing moments.

The 2/rev force and moment amplitudes for the X8 when Φ_P is varied with interference on are presented in Fig. 17. Like the interference-off case, lateral forces and moments are cancelled at the aircraft C.G., which makes sense, as the presence of aerodynamic interference does not change the symmetric nature of the vehicle. However, the 2/rev thrust, drag, and pitching moment are substantially greater, since these quantities no longer cancel within each coaxial pair. As a result, the selection of Φ_P is no longer effectively arbitrary, as the interference-off model predicted. If vibration reduction is desired, values of Φ_P near 45° are effective, even in the presence of rotor interference. Though the cancellation is not complete, the 2/rev pitching moment is reduced by 60% and the 2/rev drag force is reduced by 53%.

Fig. 18 shows the 2/rev vibratory loads as Φ_D varies with the interference on. The only substantial difference between the interference-on and off cases is the presence of large longitudinal vibratory loads, which are cancelled out at $\Phi_D = 45^\circ$. However, this comes at the cost of very large 2/rev vibrations in the lateral axis. Thus, it can be concluded that Φ_R and Φ_P are superior to Φ_D in terms of vibration reduction.

Plus Configuration

As an alternative to the X8 configuration pictured in Figs. 1 and 2, consider the "+8" configuration illustrated in Fig. 19. This platform is analogous to the "plus" configuration used in Ref. 6. In the same way that the rotor pairs of the X8 configuration were grouped into "front" and "rear" quartets, the +8 configuration's rotors can be grouped into a front, rear, and side pairs. In trimmed flight, the rear rotor pair produces the most thrust, while the front rotor produces the least, resulting in the nose-down pitching moment to maintain the nose-down attitude needed to overcome drag. Each of the side rotor pairs operate identically, producing a thrust between the rear and front pairs.

The phasing parameters available to a +8 configuration include the crossover azimuth for each pair of rotors, as well as three aircraft-level parameters. These are adapted from (Ref. 6), and illustrated in Fig. 20. Roll phasing Φ_R, causes the right rotor pairs to lead the front/rear rotor pairs (which are in-phase), while the left rotors lag by the same amount. Similarly, Φ_P causes the front/rear rotor pairs to lag/lead the side

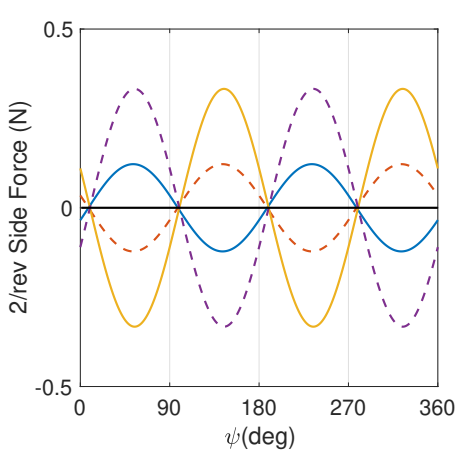

(a) 2/rev drag force at aircraft C.G., $\Phi_R = 45°$

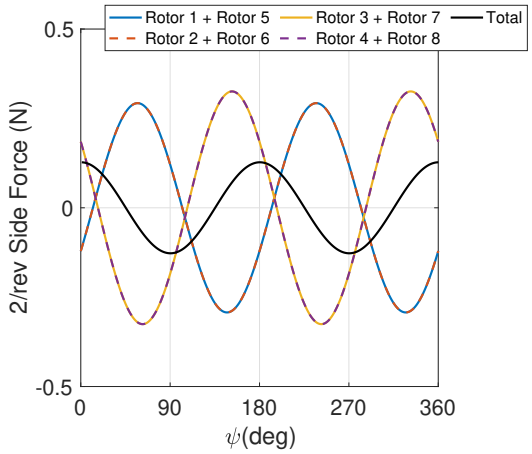

(b) 2/rev side force at aircraft C.G., $\Phi_R = 45°$

Figure 16: 2/rev drag force and side force at aircraft C.G., $\Phi_R = 45°$

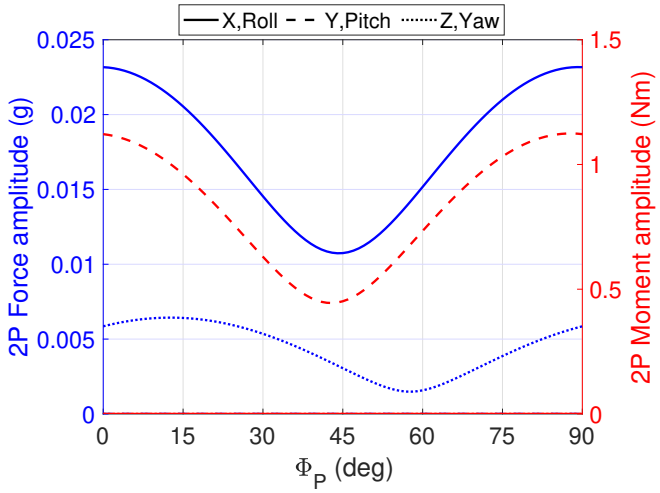

Figure 17: Amplitude of 2/rev vibratory forces and moments at aircraft C.G. using Φ_P with interference modeling

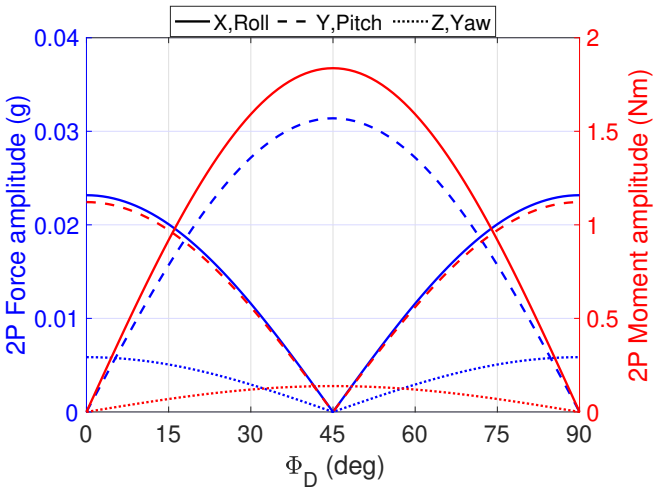

Figure 18: Amplitude of 2/rev vibratory forces and moments at aircraft C.G. using Φ_D with thrust minimizing ψ_c (V = 10m/s)

rotors, respectively. Finally, Φ_D introduces a phase difference between the left/right rotor pairs and the front/rear rotor pairs. For any Φ_D, the front rotors are in-phase with the rear rotors, and the left rotors are in-phase with the right rotors.

The +8 configuration is trimmed (with interference on) at the same 10 m/s as the X8 was, with the trim solution presented in Table 4. Naturally, the rear rotors require greater collective pitch than the side rotors, and the front rotors have the lowest collective pitch. Further, the lower rotors trim to greater collective than the upper rotors, due to the rotor-rotor interference.

Similar to cross configuration, ψ_c for each coaxial pair is chosen such that it minimizes the 2/rev thrust. Because it is most similar to the X8 configuration, consider Φ_D, the only one of the three modes that operates on all four rotor pairs at once. The 2/rev forces and moments as Φ_D is varied are plotted in Fig. 21. The behavior is qualitatively similar the between the

Table 4: Cross-configuration - Trim at 10m/s With Interference Modeling

Parameter	Value
Pitch Attitude	$-3.38°$
Front-Top Collective	$8.60°$
Side-Top Collective	$10.34°$
Rear-Top Collective	$11.35°$
Front-Bottom Collective	$9.45°$
Side-Bottom Collective	$10.4°$
Rear-Bottom Collective	$12.2°$

cross- and plus-configuration. Additionally, comparing the plus-configuration to the cross-configuration (Fig. 18) shows that the two types behave similarly as Φ_D is varied.

The 2/rev forces and moments at the aircraft C.G. using roll phasing and pitch phasing are shown in Fig. 22 and Fig. 23

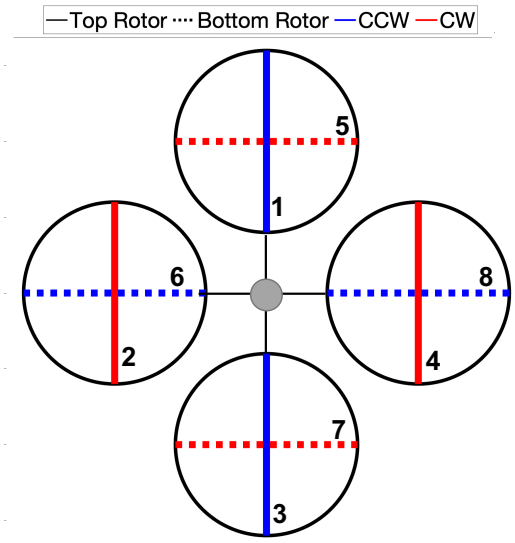

Figure 19: Plus configuration

respectively. Notably, the periodicity is between 0° and 180°, as was the case in the plus-quadcopter (Ref. 6). Additionally, in neither case is there a substantial reduction in the overall 2/rev forces and moments. In either case, reduction in force/moment in one axis will increase the force/moment in another. This is partly because these modes only operate on two of the four rotor pairs at a time, so there's always a set of two rotors that are in-phase.

To provide a more fair comparison with the X8, whose phasing modes allow the manipulation of the phase of all four rotors simultaneously, the pairs of rotors affected by Φ_P and Φ_R are considered separately. In other words, when Φ_R is varied, only the left and right rotor pairs are considered. From this, a Φ_R that minimizes the contribution of the left/right rotors to the overall vibration will be selected. This process will be repeated for Φ_P and the front/rear rotors. These solutions will be superposed on one another, and then compared to the X8.

Fig. 24 shows the 2/rev forces and moments at the C.G. for the left/right rotors only as Φ_R is varied. Because these rotor pairs spin in the same manner (i.e. the top rotor spins clockwise, and the bottom rotor spins counterclockwise), both the lateral and longitudinal forces are in-phase when the rotors are. Similarly, the hub moments are also in-phase. As a result, the majority of the forces and moments are cancelled when $\Phi_R = 45°$. The only exception is the yaw moment, which is dominated by the 2/rev drag times the moment arm. Because the 2/rev drag is out-of-phase on opposite sides of the C.G., the induced yaw moment reaches a local maximum near $\Phi_R = 45°$.

Fig. 25 shows the 2/rev vibratory loads produced by the front/rear rotor pairs as Φ_P is varied. Due to the fact that these rotors are operating at different collective pitch, there is no value of Φ_P that causes all of the vibratory loads to be small. Most of them, however, reach a minimum value near 45°. As was the case with Φ_R, the only load that is not at or neat a minimum at 45° is the yaw moment, which is dominated by

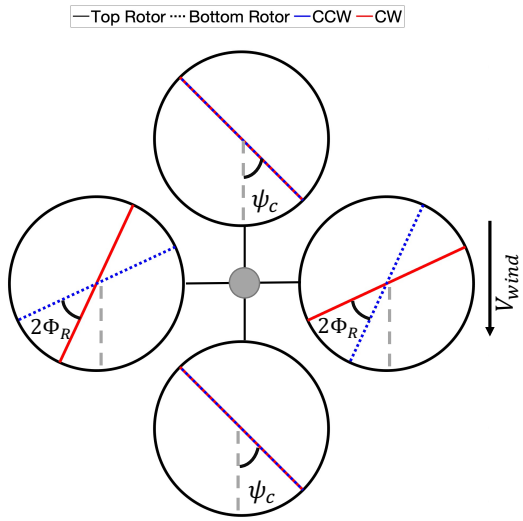

(a) Roll Phasing, Φ_R

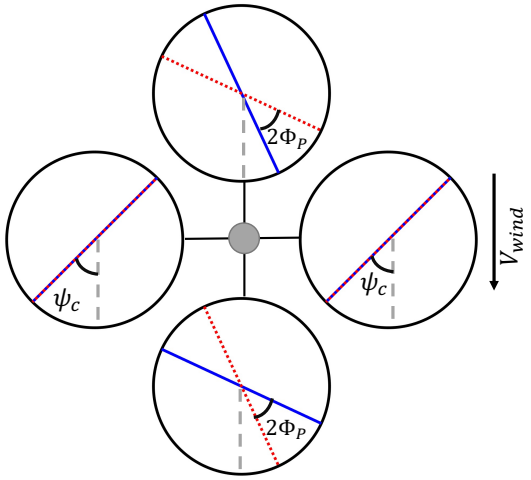

(b) Pitch Phasing, Φ_P

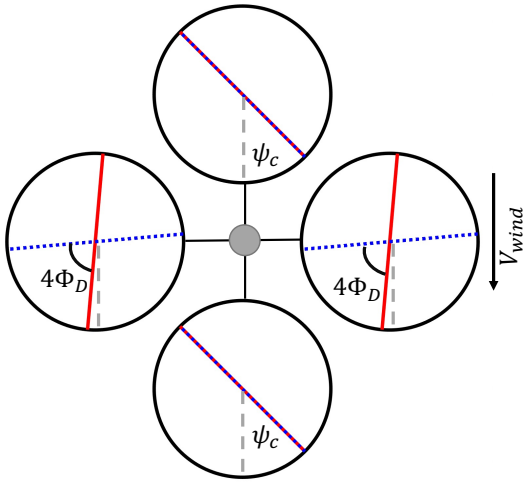

(c) Differential Phasing, Φ_D

Figure 20: Phasing Modes in Plus-Configuration

the 2/rev side-force. When the side-force of the front/rear rotor pairs is in-phase, their induced yaw moments are out-of-

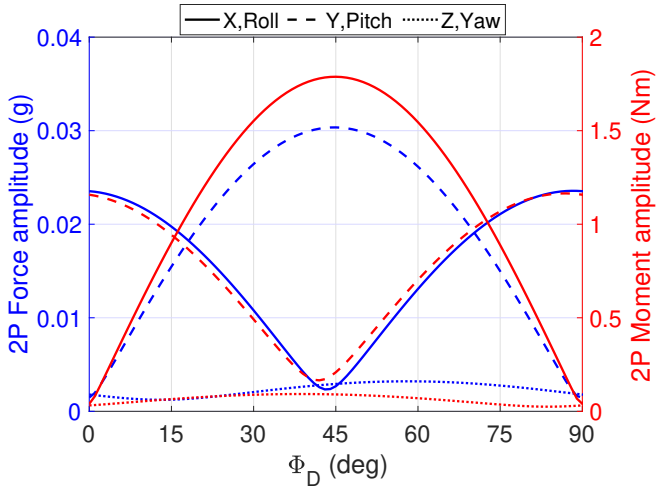

Figure 21: Amplitude of 2/rev vibratory forces and moments at aircraft C.G. using Φ_R with thrust minimizing ψ_c, Plus - configuration

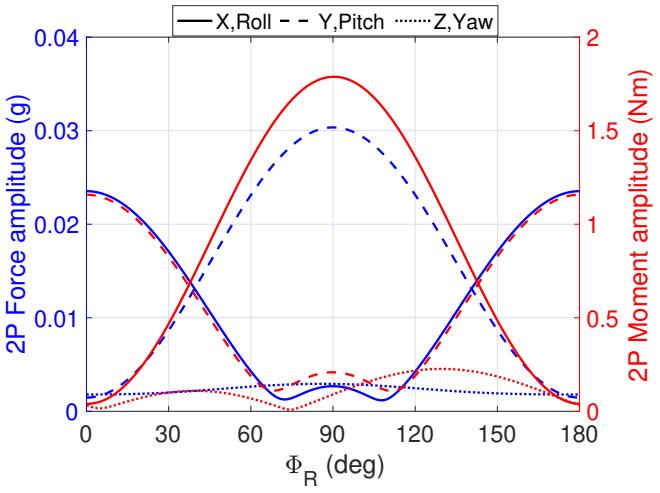

Figure 22: Amplitude of 2/rev vibratory forces and moments at aircraft C.G. using Φ_R with thrust minimizing ψ_c, Plus - configuration

phase, and vice-versa (note that the minimum of the red dotted line is near the maximum of the blue dashed line in Fig. 25.

Fig. 26 shows the magnitude of the (vector) summed 2/rev force and moment amplitudes for the corss- and plus-configuration with Φ_R and Φ_P alone, as well as with Φ_R and Φ_P superimposed.

CONCLUSIONS

Vibratory forces and moments produced by a 4kg coaxial quadcopter (in X8 and +8 configurations) equipped with fixed-RPM, variable-pitch rotors in forward flight were systematically explored by parametrically phasing the rotors relative to one another. The effect of aerodynamic interference between the rotors of a coaxial pair was examined by comparing vibration predictions with a Peters-He model (for isolated rotors), or pressure potential superposition inflow modeling (for interfering rotors).

Rather than defining the phasing of the rotors individually, a set of seven multi-rotor phase parameters were defined. Four of them were associated with individual coaxial pairs, and varying them influenced the azimuthal locations of the crossover points, where the upper and lower rotors' blades pass directly above one another. Whether or not interference was included, setting $\psi_c = 0°$ tended to minimize the 2/rev lateral loads (side force, rolling moment, and yaw moment) produced by a coaxial pair, while moderate values of ψ_c tended to reduce 2/rev longitudinal loads (drag, thrust, and pitching moments). When interference is neglected, $\psi_c = 45°$ resulted in complete cancellation of the 2/rev longitudinal loads, regardless of the thrust produced by the rotor pair. However, when interference is included, the longitudinal loads cannot be simultaneously minimized. Not only this, but the crossover at which the 2/rev thrust is minimized increases slightly as the steady thrust does. For the sake of minimizing overall vibratory moments at the C.G. (which are dominated by the thrust),

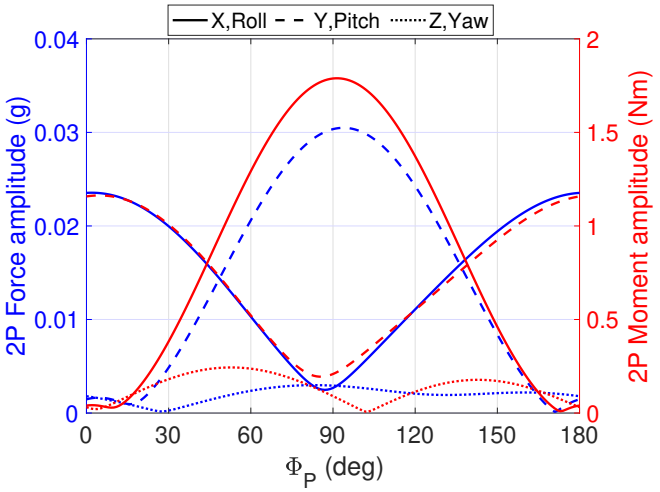

Figure 23: Amplitude of 2/rev vibratory forces and moments at aircraft C.G. using Φ_P with thrust minimizing ψ_c

ψ_c was chosen for each rotor pair such that the 2/rev thrust was minimized.

The three phase parameters left after defining ψ_c for each coaxial pair, a set of three aircraft-level parameters were defined, defined similarly to the parameters defined in Ref. (Ref. 6) for the X8 configuration. When interference is neglected, 2/rev vibrations were very low for any value of Φ_R or Φ_P, as long as the other was set to zero, though this is especially true for Φ_P. However, when interference was included, the inability to cancel longitudinal loads within a rotor pair resulted in substantially higher aircraft vibration, though using $\Phi_R = 45°$ resulted in the left/right sides of the vehicle completely canceling longitudinal loads, while there was near cancellation between the front and rear pairs for the lateral loads.

Similar phasing modes were defined on the +8 configuration multicopter, and parametrically varied. The vibrations are

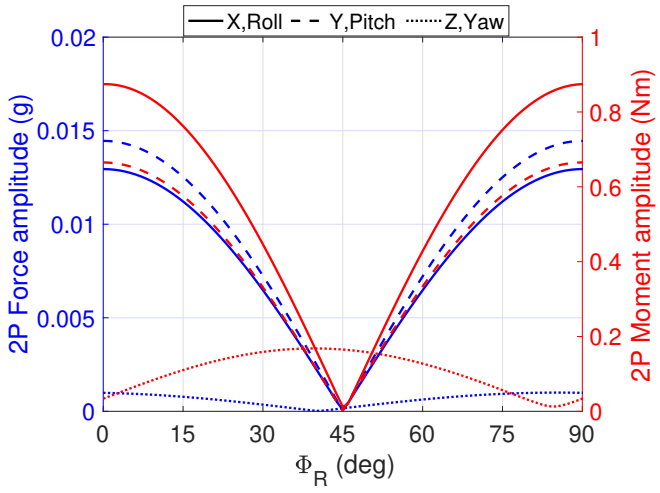

Figure 24: Amplitude of 2/rev vibratory forces and moments at aircraft C.G. using Φ_R neglecting contributions from front and rear rotors

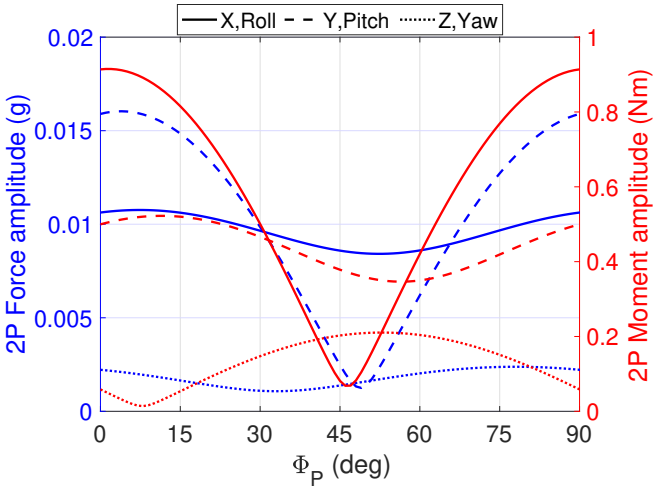

Figure 25: Amplitude of 2/rev Vibratory Forces and Moments at aircraft C.G. using Φ_P neglecting contributions from side rotors

overall higher when compared to cross-configuration. However, using Φ_P, and Φ_R simultaneously leads to a reduction of vibratory forces and moments, compared to cases where either of the phasing modes is varied. Comparing the 2-norm of 2/rev forces and 2/rev moments for all the cases analysed in this study, cross-configuration with $\Phi_R = 45^\circ$ minimizes the vibrations at the aircraft C.G.

Author contact:

Gaurav Makkar	makkag@rpi.edu
Robert Niemiec	niemir2@rpi.edu
Farhan Gandhi	gandhf@rpi.edu

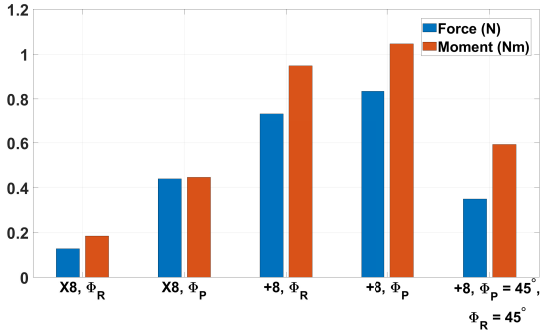

Figure 26: Comparison of total 2/rev force and moment for X8 and +8 configuration

REFERENCES

1. Holden, J., and Goel, N., "Fast-forwarding to a future of on-demand urban air transportation (Uber Elevate)," *San Francisco, CA*, 2016.

2. Swartz, K., "NASA Embraces Urban Air Mobility," Vertiflite magazine, Jan-Feb 2019.

3. Russell, C., Jung, J., Willink, G., and Glasner, B., "Wind tunnel and hover performance test results for multicopter UAS vehicles," American Helicopter Society 72nd annual forum, West Palm Beach, FL, May 2016.

4. Malpica, C., and Withrow-Maser, S., "Handling Qualities Analysis of Blade Pitch and Rotor Speed Controlled eVTOL Quadrotor Concepts for Urban Air Mobility," VFS International Powered Lift Conference, 2020.

5. Niemiec, R., Gandhi, F., Lopez, M. J., and Tischler, M. B., "System Identification and Handling Qualities Predictions of an eVTOL Urban Air Mobility Aircraft Using Modern Flight Control Methods," Vertical Flight Society 76th Annual Forum, 2020.

6. Kopyt, N., Niemiec, R., and Gandhi, F., "Quadcopter Rotor Phasing for Minimization of Aircraft Vibratory Loads," Vertical Flight Society's Transformative Vertical Flight Forum, San Jose, CA, 2020.

7. Niemiec, R., Gandhi, F., and Kopyt, N., "Relative Rotor Phasing for Multicopter Vibratory Load Minimisation," *The Aeronautical Journal*, 2021, pp. 1–20. DOI: 10.1017/aer.2021.94

8. Schiller, N., Pascioni, K., and Zawodny, N., "Tonal Noise Control using Rotor Phase Synchronization," 75th Annual Forum of the Vertical Flight Society, Philadelphia, PA, 2019.

9. Pascioni, K., and Rizzi, S. A., "Tonal Noise Prediction of a Distributed Propulsion Unmanned Aerial Vehicle," 2018 AIAA/CEAS Aeroacoustics Conference, 2018.

10. Smith, B., Gandhi, F., and Niemiec, R., "A Comparison of Multicopter Noise Characteristics with Increasing Number of Rotors," Vertical Flight Society 76th Annual Forum & Technology Display, 2020.

11. "Ehang 216," https://evtol.news/ehang-216/, [Online; accessed 15 April 2022].

12. "Phenix Flight Testing Coaxial eVTOL Drone," https://www.ainonline.com/aviation-news/defense/2022-03-10/phenix-flight-testing-coaxial-evtol-\drone, [Online; accessed 15 April 2022].

13. Niemiec, R., and Gandhi, F., "Development and Validation of the Rensselaer Multicopter Analysis Code (RMAC): A Physics-Based Comprehensive Modeling Tool," 75th Annual Forum of the Vertical Flight Society, Philadelphia, PA, 2019.

14. Peters, D. A., Boyd, D. D., and He, C. J., "Finite-state induced-flow model for rotors in hover and forward flight," *Journal of the American Helicopter Society*, Vol. 34, (4), 1989, pp. 5–17.

15. Kong, Y., Prasad, J., and Peters, D., "Development of a Finite State Dynamic Inflow Model for Coaxial Rotor using Analytical Methods," American Helicopter Society 73rd Annual Forum, Fort Worth, TX, 2017.